



A Study of Time-Dependent and Anisotropic Effects on the Deformation Response of Two Flywheel Designs

Atef F. Saleeb
University of Akron, Akron, Ohio

Steven M. Arnold
Glenn Research Center, Cleveland, Ohio

Nasser R. Al-Zoubi
University of Akron, Akron, Ohio

The NASA STI Program Office . . . in Profile

Since its founding, NASA has been dedicated to the advancement of aeronautics and space science. The NASA Scientific and Technical Information (STI) Program Office plays a key part in helping NASA maintain this important role.

The NASA STI Program Office is operated by Langley Research Center, the Lead Center for NASA's scientific and technical information. The NASA STI Program Office provides access to the NASA STI Database, the largest collection of aeronautical and space science STI in the world. The Program Office is also NASA's institutional mechanism for disseminating the results of its research and development activities. These results are published by NASA in the NASA STI Report Series, which includes the following report types:

- **TECHNICAL PUBLICATION.** Reports of completed research or a major significant phase of research that present the results of NASA programs and include extensive data or theoretical analysis. Includes compilations of significant scientific and technical data and information deemed to be of continuing reference value. NASA's counterpart of peer-reviewed formal professional papers but has less stringent limitations on manuscript length and extent of graphic presentations.
- **TECHNICAL MEMORANDUM.** Scientific and technical findings that are preliminary or of specialized interest, e.g., quick release reports, working papers, and bibliographies that contain minimal annotation. Does not contain extensive analysis.
- **CONTRACTOR REPORT.** Scientific and technical findings by NASA-sponsored contractors and grantees.

- **CONFERENCE PUBLICATION.** Collected papers from scientific and technical conferences, symposia, seminars, or other meetings sponsored or cosponsored by NASA.
- **SPECIAL PUBLICATION.** Scientific, technical, or historical information from NASA programs, projects, and missions, often concerned with subjects having substantial public interest.
- **TECHNICAL TRANSLATION.** English-language translations of foreign scientific and technical material pertinent to NASA's mission.

Specialized services that complement the STI Program Office's diverse offerings include creating custom thesauri, building customized databases, organizing and publishing research results . . . even providing videos.

For more information about the NASA STI Program Office, see the following:

- Access the NASA STI Program Home Page at <http://www.sti.nasa.gov>
- E-mail your question via the Internet to help@sti.nasa.gov
- Fax your question to the NASA Access Help Desk at 301-621-0134
- Telephone the NASA Access Help Desk at 301-621-0390
- Write to:
NASA Access Help Desk
NASA Center for Aerospace Information
7121 Standard Drive
Hanover, MD 21076



A Study of Time-Dependent and Anisotropic Effects on the Deformation Response of Two Flywheel Designs

Atef F. Saleeb
University of Akron, Akron, Ohio

Steven M. Arnold
Glenn Research Center, Cleveland, Ohio

Nasser R. Al-Zoubi
University of Akron, Akron, Ohio

Prepared for the
14th Symposium on Composite Materials: Testing and Design
sponsored by the American Society for Testing and Materials
Pittsburgh, Pennsylvania, March 11–12, 2002

National Aeronautics and
Space Administration

Glenn Research Center

Acknowledgments

Prof. Saleeb and Dr. Al-Zoubi would like to acknowledge the financial support provided by NASA Glenn Research Center, under research Grant NCC3-788 to the University of Akron, for this work.

Trade names or manufacturers' names are used in this report for identification only. This usage does not constitute an official endorsement, either expressed or implied, by the National Aeronautics and Space Administration.

Available from

NASA Center for Aerospace Information
7121 Standard Drive
Hanover, MD 21076

National Technical Information Service
5285 Port Royal Road
Springfield, VA 22100

Available electronically at <http://gltrs.grc.nasa.gov>

A Study of Time-Dependent and Anisotropic Effects on the Deformation Response of Two Flywheel Designs

Atef F. Saleeb
University of Akron
Civil Engineering Department
Akron, Ohio 44325

Steven M. Arnold
National Aeronautics and Space Administration
Glenn Research Center
Cleveland, Ohio 44135

Nasser R. Al-Zoubi
University of Akron
Civil Engineering Department
Akron, Ohio 44325

Abstract: The influence of material time dependency and anisotropy in the context of two specific flywheel designs—preload and multi-directional composite (MDC)—is investigated. In particular, we focus on the following aspects: 1) geometric constraints, 2) material constraints, 3) loading type, and 4) the fundamental character of the time-dependent response, i.e., reversible or irreversible. The bulk of the results presented were obtained using a composite (PMC IM7/8552 @135 °C) material system. The material was characterized using a general multimechanism hereditary (viscoelastoplastic) model. As a general conclusion, the results have clearly shown that both the preload and the MDC rotor designs are significantly affected by time-dependent material behavior, which may impact the state of rotor balance and potentially reduce its operating life. In view of the results of the parametric studies and predictions made in the present study, the need for actual experimentation focusing on the time-dependent behavior of full-scale flywheel rotors is self-evident.

Introduction

General

Flywheels, for well-known reasons, are extensively used as efficient energy storage systems. Among many different designs, several are being assessed employing different material systems, with greater demands on the repeated spinning (up/down) type of loading. To date, the bulk of analytical/numerical studies have been made on the time-independent response of these systems, identifying the key factors as: interference fit (also known as misfit), mean radius, thickness, material-property- and/or load-gradation, and speed, all of which must be simultaneously optimized to achieve the “best” and most reliable design [1]. Alternatively, comparatively few studies are

available on the effect of time dependency in flywheel applications, with the majority of those conducted making use of classical viscoelasticity, i.e., hereditary-integral type assumption, [2-11]. Further complications, arise from the fact that despite the ample evidence of various types of material time dependency, particularly for PMC systems [12-19]; the underlying fundamental character of the time-dependent behavior (i.e., reversible vs. irreversible) and its ramifications (through constitutive modeling) in structural applications (e.g., flywheels) has not been carefully examined and critically assessed. For instance, in PMC literature, the irreversibility of the material is often masked by such practices as mechanically conditioning the material, e.g., prior to creep/creep-recovery tests, or subtraction of the permanent strain from the creep recovery data, etc.; thus justifying the utilization of a predetermined simplified constitutive theory, for example linear or nonlinear viscoelasticity, [17-19].

Knowing that for space applications (e.g., the International Space Station, ISS) a flywheel must operate for an extended period of time (approximately 15 years) at moderate temperatures (i.e., 90 – 135 °C) and since it is important that both stress and deformations not reach any critical limits during the life span of the rotor, a further investigation and study into the influence of time dependency and anisotropy effects in the context of a given design is required. This provides the main motivation for the present work.

Objectives, Scope, and Outline

The main objective here is to provide a complementary study, to our previous time-independent investigation [1], that focuses on the effects of time dependency in material behavior and its ramifications. In particular, emphasis is placed on investigating the following aspects: 1) geometric constraints; such as limiting plane stress/strain conditions; 2) material constraints, resulting from strong anisotropy (e.g., due to inclusion of elastic fiber reinforcement in the composite rotor) as well as possible material-property gradation; 3) loading type, i.e., steady vs. cyclic; and 4) the implications of the underlying fundamental character of the time-dependent response, i.e., reversible (viscoelasticity-solid representation) or the more general irreversible viscoelastoplastic- representation.

To limit the scope, two specific rotor designs are considered: 1) preload (filament wound) type (single disk and multiple disk) and 2) Multi Directional Composite (MDC) or laminated type. For both designs, the use of a solid hub with interference fit will be considered (even though other hub configurations such as growth-matching, etc, are known to provide important alternatives). Furthermore, to better isolate the role played by the effect of the material's time dependency; we have elected to keep "frozen" certain other design parameters. In particular, the mean radius ($R_m = 10.16$ cm) of the solid hub-rotor design, the in-plane thickness, as well as the amount of interference fit preload (an "equivalent" initial hoop strain of 0.5%) will be kept at their selected (prototypical) values in all the results reported here. However, it is emphasized that the significant effects (especially quantitative) due to changes in these "frozen" variables will certainly persist in the time-dependent domain, as they did in the purely elastic case, [1].

The majority of the present study will involve a highly anisotropic polymer matrix composite (PMC) material system known as IM7/8552 [20] and will be performed at

one *constant* elevated temperature, i.e., 135 °C. This temperature is considered to be at the high end of the operational temperature range for this material, hence leading to significant time dependency. However, some solutions have also utilized an isotropic metallic alloy and some “artificial” variants (wherein “stiff” elastic fibers are envisioned to be embedded) to complete our parametric studies. Also note that many (if not all) of the features and phenomena investigated herein will be even further enhanced under nonisothermal conditions for the flywheel systems.

With the rather complex nature of time-dependent calculations (i.e., requiring a detailed time-marching strategy) the format of the presentation of results becomes important in evaluating the alternative designs. Here we have opted to focus on two major aspects: 1) spatial distribution over the rotor domain (in-plane and/or out-of-plane) of representative stress/strain type quantities, and 2) temporal evolutions of the quantity of interest for a selected location.

An outline of the remainder of the paper is as follows. We start by outlining the main ingredients of the time-dependent material model employed, together with its characterization. In the next section, the solution procedure is presented, including the finite element (FE) discretization, and the description of the prototypical load history. To this end both the global structural and local (constitutive/integration point) calculations and validation problems are also briefly described. The analysis results for a preloaded design composed of either a viscoelastic or viscoelastoplastic rotor are then presented. These results provide the basis for assessing the effects of: 1) material representation, 2) material constraints, 3) geometric constraints, and 4) material gradation. Following, the analysis results of the more complex MDC design (using the viscoelastoplastic material characterization of the IM7/8552 system) are presented for both in-plane and out-of-plane response components. Finally, the main conclusions of the study are listed.

Time Dependent Material Representation

Material Model

Here, we consider a macroscale approach (wherein coupon level testing is utilized and not micromechanics) to determine the deformation and life behavior of a composite material. The specific material model employed in the analysis is derived from a complete potential-based formulation accounting for nonlinear kinematic hardening and elastic-recovery mechanisms. This model has been successfully applied to metallic materials, for details, the reader is referred to references [21-24].

The resulting general multi-mechanism hereditary model (Fig. 1) partitions the total strain into two major response components: 1) a reversible/linear viscoelastic and 2) an irreversible/nonlinear viscoplastic component. Moreover, both of these representations can be either activated or suppressed, thus enabling special representations depending on the required or anticipated material behavior (e.g., purely elastic or viscoelastic, elastic-viscoplastic, perfectly-viscoplastic-with no hardening/recovery, etc.). In the case of reversible (viscoelastic) behavior the character of the response remains the same with time and the solution can be confined between two limiting cases. On the other hand, in the irreversible (viscoplastic) representation the response can change its character with time whenever permanent deformation

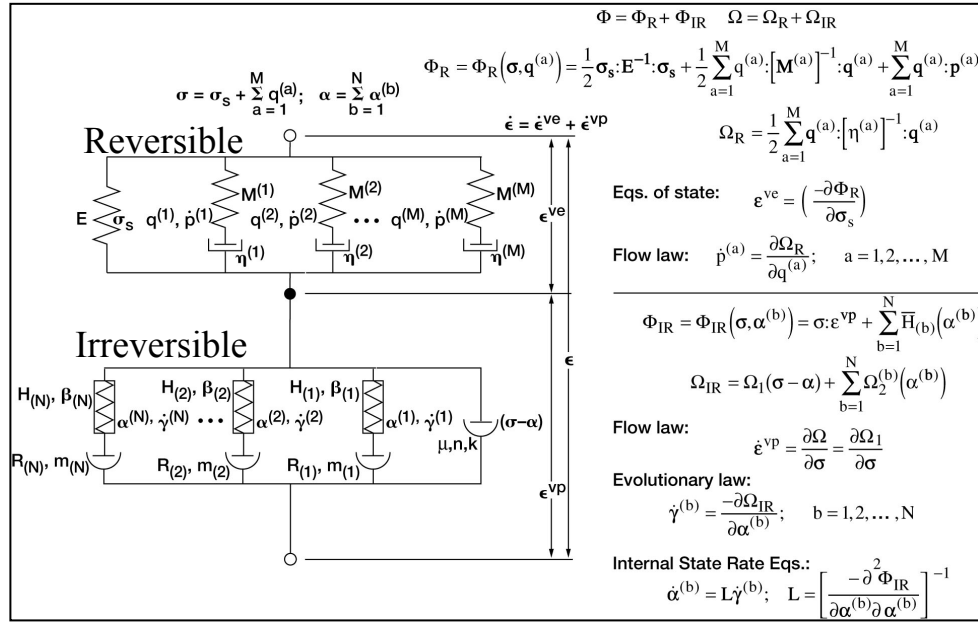


Figure 1 - Representation of a general multimechanism hereditary formulation.

dominates. For example, in the case of 1) passing from transient to steady state creep or 2) increasing inelastic strain cycle by cycle (a phenomenon known as material ratchetting) and/or shakedown (wherein the material stops deforming inelastically).

The above general viscoelastoplastic framework, provides a convenient means for consistently interpreting general hereditary behavior. This is particularly true in connection with the long-standing history of time-dependent constitutive representation attempts for PMC systems (both thermoset and thermoplastic polymeric matrices). This work, both analytical and experimental, which spans more than three decades [12- 19, 25, 26], has focused on the study of the changes in mechanical properties (e.g., stiffness moduli and strength) as a function of time (i.e., from the glassy to the transition and rubbery states) under conditions of uniaxial creep and monotonic constant strain rate loading, be they tensile or compressive. Essentially, all types of reversible and irreversible response histories [classified herein as 1) reversible (viscoelastic), 2) nonlinear irreversible (viscoplastic) and 3) softening/damage (e.g. matrix crazing), time-dependent behavior] have been observed to differing degrees; where typically the two types of permanent deformations resulting from (2) and (3) above, have been difficult if not impossible to isolate under simple conditions of creep with recovery and/or uniaxial monotonic loading. Consequently, this history suggests the need for a coupled viscoelastoplastic constitutive model as utilized herein. Furthermore, the neat and logical partitioning of the stored and dissipative parts of the total energy, underlying our present framework is directly applicable in the context of recent design/critical energy failure criteria for PMC systems [17, 18, 19]. Moreover, unlike some of these latter developments (e.g., the NMC and the RW approaches in reference [19]), the present framework allows for calculation of deformations beyond the “yield” point and in the post creep-rupture regimes, for some examples, see reference [24] for general coupled viscoelastoplastic-damage applications.

Furthermore, the present model directly and consistently handles the nonlinear transient/steady/cyclic creep phenomenon, thus alleviating the need for ad-hoc “pseudo-viscoplastic” representations that are sometimes used [25]. These latter representations may give rise to physically-unrealistic discontinuous strain responses due to a sudden change in the stress, or the associated unnecessary restrictions of the traditional, but rather limited, strain-hardening creep approach (see references [27, 28] for some critical limitations on this traditional approach) within the context of time-stress-superposition principle (TSSP), see references [19, 25]. Consequently, the mere fact that most high performance flywheels will be manufactured using PMC materials does not automatically eliminate the need for accounting for irreversible behavior – thus viscoplastic constitutive representations. Furthermore, the present IM7/8552 system of interest, has exhibited significant irreversible deformations, in the range of 5-17%, at multiple temperatures, see reference [20], in relatively short periods of time (days) as compared to the desired 15 year flywheel mission cycle, thus further justifying the need to perform the current parametric study, to enhance our understanding of the ramifications of time dependent material behavior.

Material Characterization

Rapid characterization of the pertinent materials using the current material model is accomplished (given experimental test results see references [20, 23]) using the constitutive parameter estimator known as (COMPARE, reference [24]) to estimate the material parameters. As alluded to earlier, two materials were used in the present analysis. The first is an isotropic titanium alloy known as TIMETAL 21S. It was characterized in an earlier study [22], at 650 °C, using the reversible viscoelastic portion of the model. Table 1 shows the resulting material parameters.

The second is a PMC material known as IM7/8552 for which experimental data, at 135 °C, is available for use in the characterization process. These experiments, which are described in detail in reference [20], include one constant-strain-rate experiment in the longitudinal direction, and in the transverse direction, three relaxation-with- unloading relaxation periods, three creep-with strain recovery, and a single cyclic (stress-controlled) test. All seven tests were conducted under compressive loading. For convenience in the present study, identical behavior in tension and compression is assumed, even though some “small” differences in tension and compression were observed experimentally [20]. The PMC was characterized using two modeling approaches; a purely viscoelastic representation (using 5 viscoelastic mechanisms), and a generalized viscoelastoplastic model (using 1 viscoelastic combined with 2 viscoplastic mechanisms). The resulting material parameters are shown in Tables 2 and 3, respectively, and the corresponding model simulations are shown in Fig. 2. Note, very good qualitative agreement between model simulation and experiment is observed given either representation.

Finally, some artificial modifications were also created to enable parametric studies to be conducted in the context of: 1) “shutting off” the time dependency in one of the material directions to simulate the influence of strong anisotropy, 2) material property gradation; by introducing a new polymer matrix with more tendency to creep, i.e., increasing the steady state creep rates over that of the given PMC system. In all the cases studied the inner solid hub was composed of titanium and assumed to be *elastic* ($E = 90 \text{ GPa}$, $\nu = 0.33$, $\rho = 5000 \text{ kg/m}^3$) due to the relatively moderate application temperature expected.

Table 1- *Final Characterized Viscoelastic Parameters Using Six Viscoelastic Mechanisms for TIMETAL 21S @ 650 °C. ($\rho=5000 \text{ kg/m}^3$)*

Material Parameter	Units	Value	Material Parameter	Units	Value
E_s	GPa	21.75	Em_4	GPa	6.523
ν	-	0.365	ρ_4	sec	9693
Em_1	GPa	41.37	Em_5	GPa	3.965
ρ_1	sec	0.5	ρ_5	sec	14460
Em_2	GPa	6.895	Em_6	GPa	3.434
ρ_2	sec	50	ρ_6	sec	28218
Em_3	GPa	21.120			
ρ_3	sec	974			

Table 2 - *Final Characterized Viscoelastic Parameters using five Viscoelastic mechanisms for PMC @ 135 °C. ($\rho=1578 \text{ kg/m}^3$)*

Material Parameter	Units	Value	Material Parameter	Units	Value
E_{11}	GPa	103.35	Em_3	GPa	2.07
E_{22}	GPa	6.047	ρ_3	sec	30×10^3
ν_{12}	-	0.2568	Em_4	GPa	11.72
G_{12}	GPa	34.47	ρ_4	sec	41080×10^3
Em_1	GPa	17.24	Em_5	GPa	2.76
ρ_1	sec	5×10^3	ρ_5	sec	292.91×10^3
Em_2	GPa	13.79			
ρ_2	sec	4×10^3			

Table 3 - *Final Characterized Viscoelastoplastic Parameters using one Viscoelastic and two Viscoplastic mechanisms for PMC @ 135 °C. ($\rho=1578 \text{ kg/m}^3$)*

Material Parameter	Units	Value	Material Parameter	Units	Value
E_{11}	GPa	147.0	m_1	-	7.177
E_{22}	GPa	9.90	m_2	-	1.057
ν_{12}	-	0.2568	β_1	-	15.723
G_{12}	GPa	68.95	β_2	-	4.00
Em	GPa	4.04	R_1	1/s	5.0×10^{-9}
ρ	sec	18.04×10^3	R_2	1/s	1.113×10^{-3}
κ	MPa	1.0	H_1	GPa	8.44
κ_1	MPa	41.37	H_2	GPa	6.05
κ_2	MPa	34.47	ζ	-	0.5
n	-	3.605	ξ	-	0.9999775
μ	GPa -s	2.45×10^5			

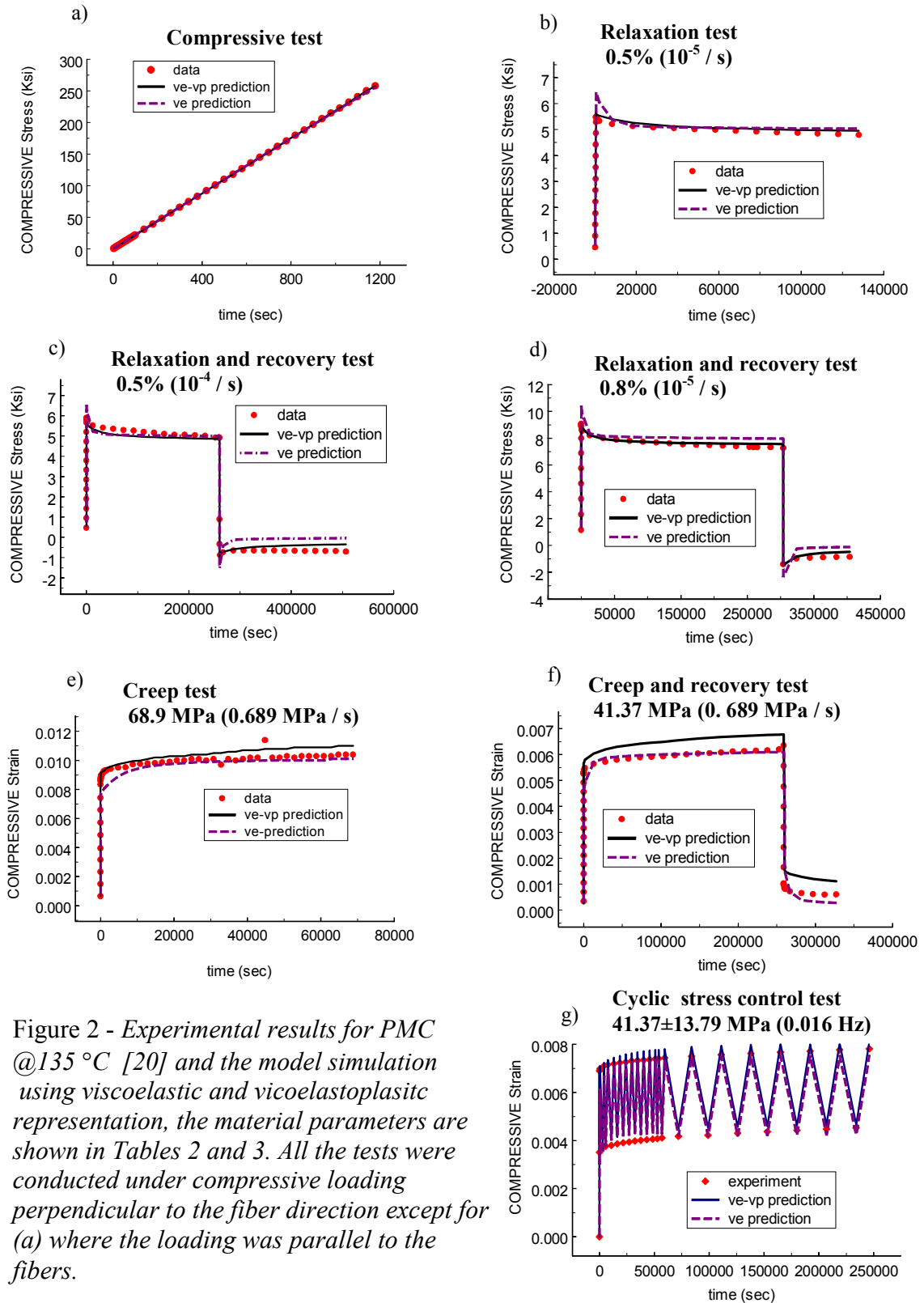


Figure 2 - *Experimental results for PMC @135 °C [20] and the model simulation using viscoelastic and viscoelastoplastic representation, the material parameters are shown in Tables 2 and 3. All the tests were conducted under compressive loading perpendicular to the fiber direction except for (a) where the loading was parallel to the fibers.*

Solution Procedure

Geometry and Meshing Discretization

Both preload and MDC designs are assumed to have the same in-plane geometry, where the inner hub is 12.7 cm in diameter, and is press fit with a concentric 7.62-cm thick composite rim (rotor), see Fig. 3a. The out-of-plane dimension is taken to be 4 times the mean radius for the preload, log, design and 5.08 cm in the MDC design. The preload design consists of one or three circumferentially reinforced rim(s), whereas

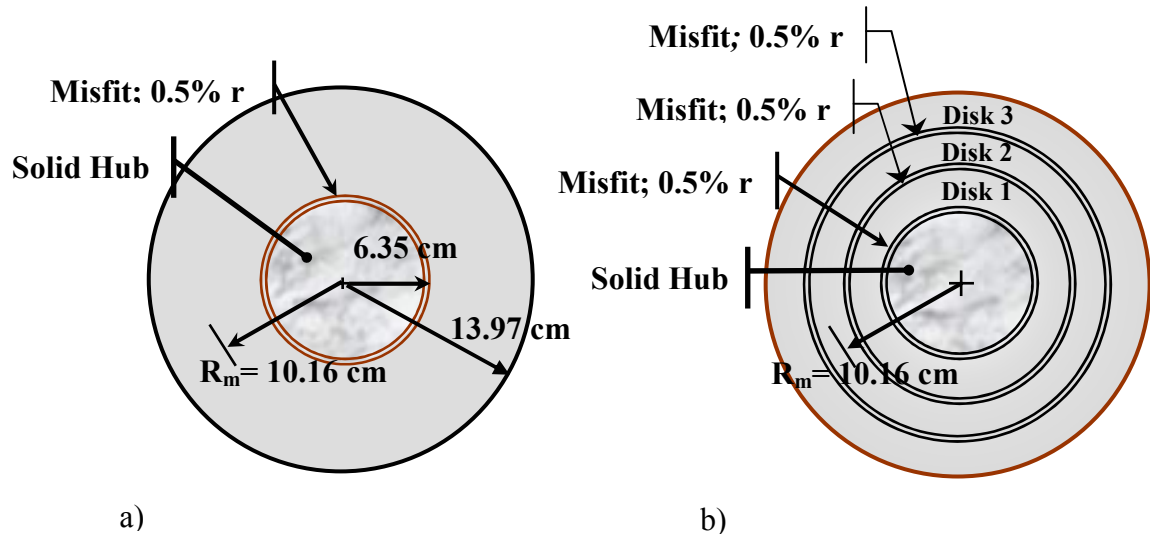


Figure 3 - Schematic representation of the: a) Hub single 7.62-cm rim, b) Hub attached to three (each 2.54-cm thick) rims.

the MDC design consists of twenty (evenly split) stacked circumferentially and radially reinforced disks. The circumferentially reinforced disks are 10 times thicker (in the out-of-plane direction) than the radially reinforced disks (thereby making a total thickness of 5.08 cm); see Fig. 4b.

The problem of a rotating disk was solved numerically using four-noded axisymmetric elements within the commercial finite element analysis software package known as, ABAQUS standard [29]. The boundary conditions and number of elements employed depended upon the different applied geometric constraints. For example, in the preload “log” configuration; i.e., three 2.54-cm thick rims (geometry shown in Fig. 3b), 80 elements were used for each rim, in addition to the solid hub elements. Furthermore, we used one column of gap elements (8 elements) at the location of each interface, as shown in Fig. 4a. In the single 7.62-cm rim configuration the same number of elements (80) was maintained for the rim. For the extreme cases of plane stress or plane strain, only one row of elements was used (20 elements, in addition to the solid hub elements). For the plane stress case, the out-of-plane dimension was reduced to 1% of the in-plane dimension), whereas in the plane strain case the out-of-plane displacements were completely restrained.

In the MDC design one row of elements were used for each of the radially reinforced layers and two rows for the circumferentially reinforced layers, thus resulting in a total of 210 axisymmetric (CAX4) elements (in addition to the solid hub and gap (INTER2A) elements) with the maximum element aspect ratio being 11. Note Fig. 4b, illustrates only half (in the out-of-plane direction) of the depth of the rotor system due to the use of symmetry. One column of gap elements was used (15 elements) between the solid hub and the composite rim elements.

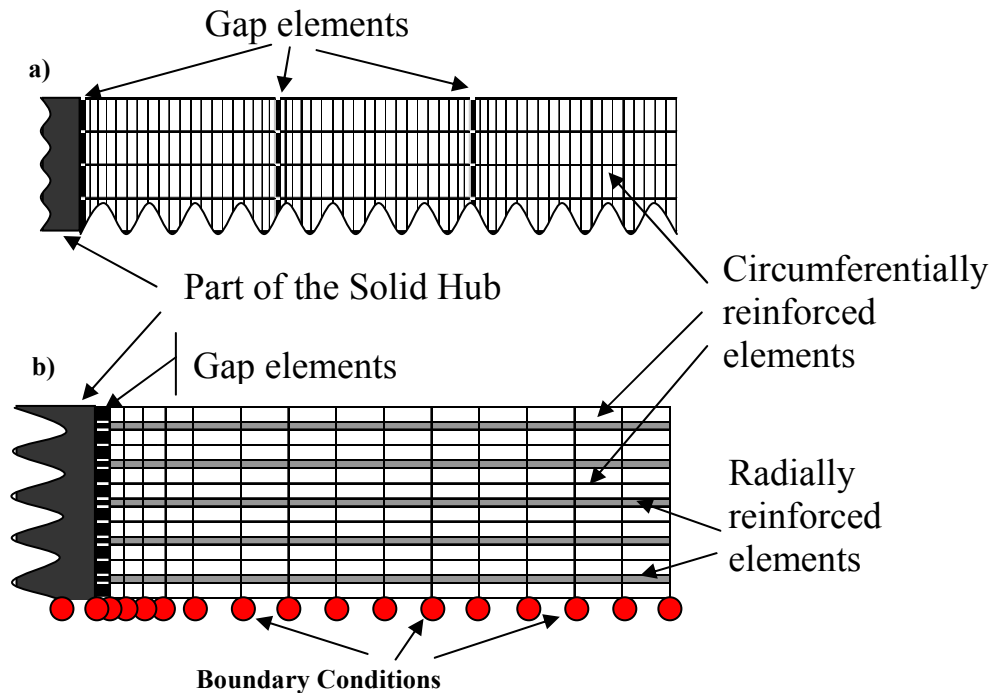


Figure 4 - Schematic representation showing the finite element (axisymmetric) mesh used in the analysis. a) A multi disk preload (log) design showing the three 2.54-cm rims and part of the hub b) MDC design showing the rim and part of the hub.

Prototypical Loads

In selecting our load cases we were guided by the anticipated service life of the ISS. That is, due to the sun/eclipse orbital constraints in addition to energy storage considerations, the flywheel rotor is expected to be spun up to 60 000 rpm within 1 hour and then down to 40 000 rpm in half an hour (Fig. 5b), with occasional deep draws to as low as 20 000 rpm. For the current study, two types of *mechanical* loading were considered, that of constant and cyclic spinning. In the former case, two limiting constant rotations (60 000 and 20 000 rpm) were used in the analysis (see Fig. 5a), whereas, the cyclic load history was taken to follow a proposed ISS mission profile, (see Fig. 5b).

The interference fit at each interface was introduced using the gap element, where the outer nodes (of the gap element) have been given a radial dimension that is less than

the inner nodes by an amount that is equal to the interference fit ($0.5\% r$), where “ r ” is the radius of the interface of interest. This value of interference fit was maintained in *all* the problems including the multi-disk preloaded design in which the three sub-rims each have a 0.5% compressive hoop prestrain imposed on them.

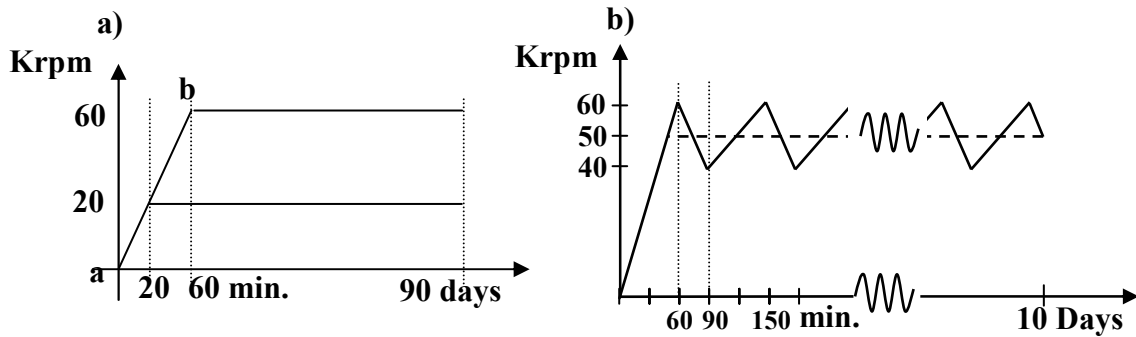


Figure 5 - Loading histories a) Constant loading. b) Cyclic loading

In addition to the mechanical loadings one case of linearly distributed *thermal* loading was used, by introducing it in two steps; initial ramp and constant loading.

Global (Time-stepping scheme) and Local (constitutive) Calculations

In both the cyclic and constant load cases, each “linear” portion of the load was considered to be a step (Fig. 5) and in each step ABAQUS’s feature of automatic global stepping was activated. As an example, the program traversed the linear loading ramp (ab in Fig. 5a) in 140 sub-increments (after limiting the automatic global stepping to be between 10^{-21} and 500 seconds) in the MDC design.

The material model was linked to the main program using the UMAT (user material-definition) option within ABAQUS where the various material properties are identified within the input file. Detailed constitutive level calculations (stress-update/stiffness, etc.) within the UMAT routine were developed using an implicit integration technique, see references [22, 24] for details.

Validation Problems

Different problems were successfully solved which validated the constitutive model implementation within ABAQUS as well as the overall solution procedure. To this end a comparison was made with an existing analytical solution for different loading and geometric cases. Secondly, the linear viscoelastic solution was compared to the “proven” elastic limit solutions; i.e., instantaneous limit (dynamic modulus) and equilibrium/ steady-state (static modulus) at “infinite times”, see reference [1, 23]. Lastly, results using the viscoplastic model and the “finite-height,” log, geometric model demonstrated that the solution was bounded by the two limiting plane-stress/ plane-strain cases, as one would expect.

Analysis Results for Preload Design

Material Representation

The influence of the material representation (be it elastic (reversible) or plastic (irreversible) like) on the stress analysis is presented here.

Characteristic Highlights of a Viscoelastic Solution Given a Single, Isotropic, Disk- In this study a single disk (with an “infinitely-soft” hub and a TIMETAL 21S rim) was subjected to two different load types. Both of the loads were held constant over the applied time; a linear thermal load distribution (from 310° C at the OD to 0° C at the ID) and an applied rotational speed. Results indicate that in the thermal loading case, the multiaxial strain state is constant while the stress state changes with time. Alternatively, in the mechanical load case, the stress state is constant in time while the strain state evolves with time. Thus both strain-controlled and stress-control test conditions are simulated, respectively. In the two cases the initial (instantaneous response) and final (infinite time) states were obtained from the elastic analysis using the upper stiffness limit ($D = \Sigma M_i + E_s$) and the lower stiffness limit (E_s), respectively. This fact places the actual viscoelastic solution, at anytime, within these two limits, see Fig. 6a and b. For convenience in reporting our stress results in Fig. 6 and all subsequent figures, we have utilized a normalization factor (denoted as N.F.) in each individual figure corresponding to the purely elastic solution.

Fundamental Differences Between a Viscoelastic and Viscoplastic Solution- A major difference between the two material representations is clearly displayed when the “unloading” portion of the experimental response is examined, see Fig. 2c and 2d as well as reference [20]. Here the viscoelastic solution shows complete recovery/reversible behavior (no permanent residual stress) and the viscoelastoplastic representation show some remaining residual stress (non-recoverable behavior) as does the experimental data.

On the structural level, the titanium hub fitted with a PMC rim was subjected to cyclic loading and in another case to a constant “average” load equal to the mean of the cyclic load case, Fig. 5b. The problem was analyzed using the two material representations, i.e. viscoelastic and viscoelastoplastic. Clearly, the results of the viscoelastic analysis show that the “average” constant load response coincides with the mean cyclic loading response, Fig. 7a as one might intuitively expect. In the viscoelastoplastic case, however the two responses deviate, in that the cyclic loading shows more time dependency than does the constant load profile, as seen in (Fig. 7b). This deviation (which was captured by the viscoelastoplastic behavior model) comes from the accumulation of inelastic strain during each cycle; i.e., ratchetting phenomenon. This ratchetting phenomenon represents another major difference between the two material representations. Obviously, this difference in fundamental behavior under cyclic conditions suggests the urgent need to accurately determine experimentally the appropriate multiaxial representation for this material. This is because; if the material were “plastic” in nature significant accumulation of stress/strain could be (depending on the stress level) encountered over time, which is in, stark contrast to that obtained from essentially an “elastic” material. Note, to the authors knowledge, no experimental data on the ratchetting behavior of flywheel system is currently available.

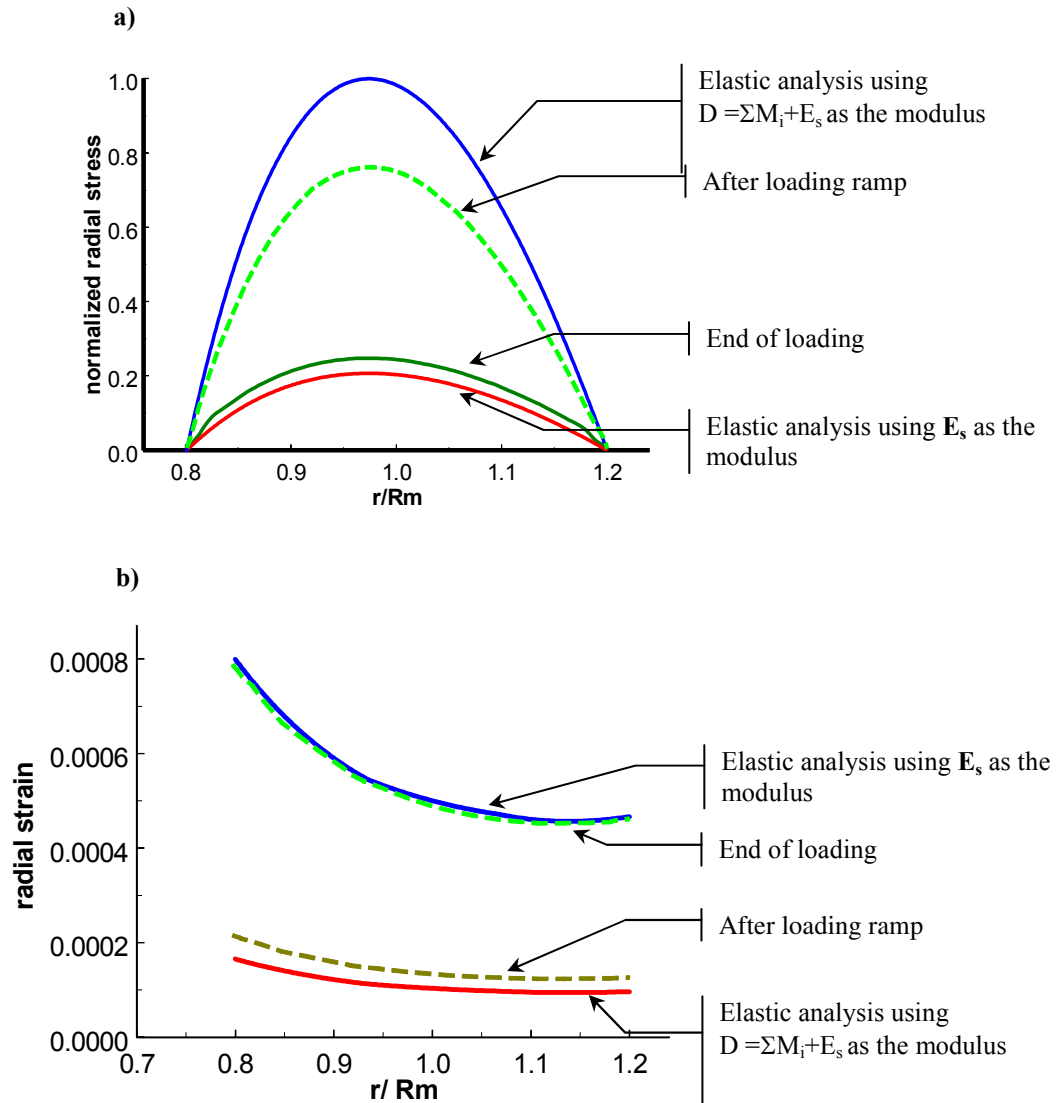


Figure 6 - Viscoelastic response of a single (TIMETAL 21S) disk with extremely soft hub. a) Normalized radial stress after subjecting the disk to constant thermal loading (linear temperature distribution), $N.F.=1.67$ MPa. b) Radial strain distribution after subjection to constant rotational speed. $R_m=19.05$ cm.

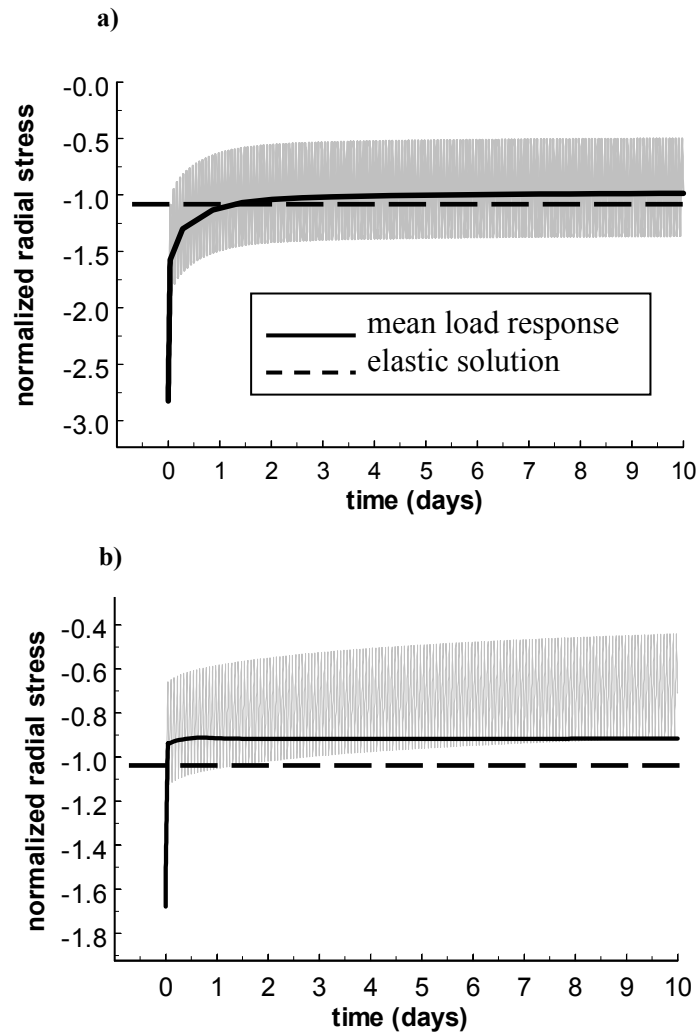


Figure 7 - Comparison between cyclic rotation between 60 and 40 Krpm and that of an average rotation of 50 Krpm. a) Using viscoelastic analysis. b) Using viscoelastoplastic analysis. $N.F.=82.7$ MPa.

Material Constraints

Here, three different “artificial” modifications in material behavior (starting from an isotropic steel alloy at elevated temperature) were imposed so as to study the influence of material constraint in the context of a thin (plane stress), interference fit, hub-rim design. In the first case an isotropic metallic like material was used in the rim. This was then compared to a second case in which the rim was composed of a “composite” made out of the same matrix material but that was reinforced circumferentially with stiff elastic fibers. In the third case the same isotropic matrix was used as in the first case, but now with the stiff elastic fibers assumed to be in the radial direction. All three systems were subjected to the same constant rotation and analyzed with the same viscoplastic model, but with correspondingly different fictitious material parameters. Figure 8 shows the history of the interfacial stress (contact pressure) for the three different material cases normalized with the elastic matrix solution. The figure shows that the isotropic case exhibits the greatest loss of preload (due to time dependency), followed by the case of radial and then circumferential fiber reinforcement. Given circumferential reinforcement, very little time dependency was observed. Indeed, it is this latter favorable situation that provides the appeal of circumferential filament-wound designs in practice.

Geometric Constraints

From the standpoint of practical designs, the ratio of “height” (out-of-plane) to in-plane mean radius of the rotor can vary significantly. The two limiting extremes of plane strain and plane stress conditions, however, correspond to a very high and very low ratio, respectively. These limiting cases were studied in the context of a single PMC rim/hub design, subjected to three different constant rotational speeds (zero, 20 000 and 60 000 rpm) for 90 days given a viscoelastoplastic material model representation.

The results show that in all three cases the plane stress condition (thin disk case) exhibited more time dependency than did the plane strain case when referring to loss of preload (i.e., the radial stress distribution; see Fig. 9). For both geometric constraint conditions, most of the time-dependent losses (in the interfacial pressure) occur during the loading ramp, given the rather high-assumed operational temperature of 135 °C for the present PMC system and the relatively slow loading ramp rate. Clearly, the no rotation case (simulating a flywheel being stored at elevated temperature) shows the most severe loss in preload pressure (33% in plane stress, 10% in plane strain after 90 days), Fig. 9a and b and illustrates why one would not want to store a given flywheel system at elevated temperatures. For the case of 60 000 rpm (Fig. 9e and f) the influence of time dependence does not appear to be as prevalent as in the other two load cases – since at the interfacial location between the hub and rim the radial stress state is equal to that of the elastic solution. Be not deceived, however, time dependency does exist in that region especially during the loading ramp (when the compressive stress level is high), but due to the high rotational spin up speed the maximum stress level is shifted to the location of the mean radius; wherein, a positive stress state exists and stress relaxation is noticeable, especially in the plane stress case.

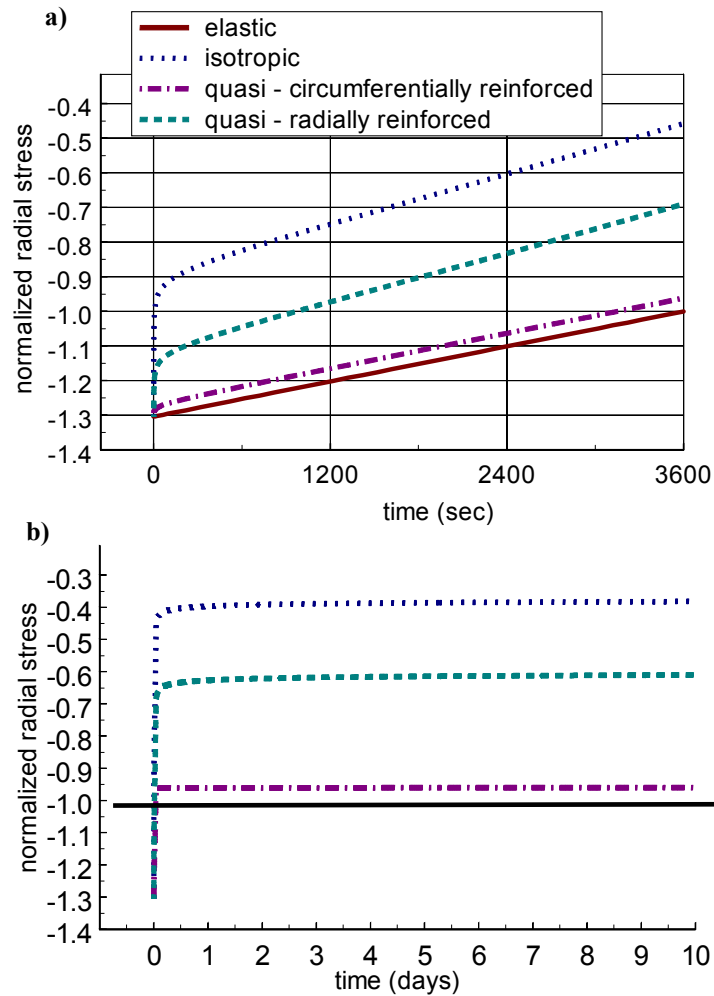


Figure 8 - Viscoplastic analysis of rotating hub-disk (a 0.5% hoop prestrain) with constant speed for three different fictitious materials; case 1 is isotropic, in case 2 the radial direction is semi-prevented from creeping and in case 3 the circumferential direction is semi-prevented from creeping. a) represents the history of the interfacial pressure during the loading ramp; whereas b) represents the entire interfacial pressure history. $N.F.=206.1$ MPa.

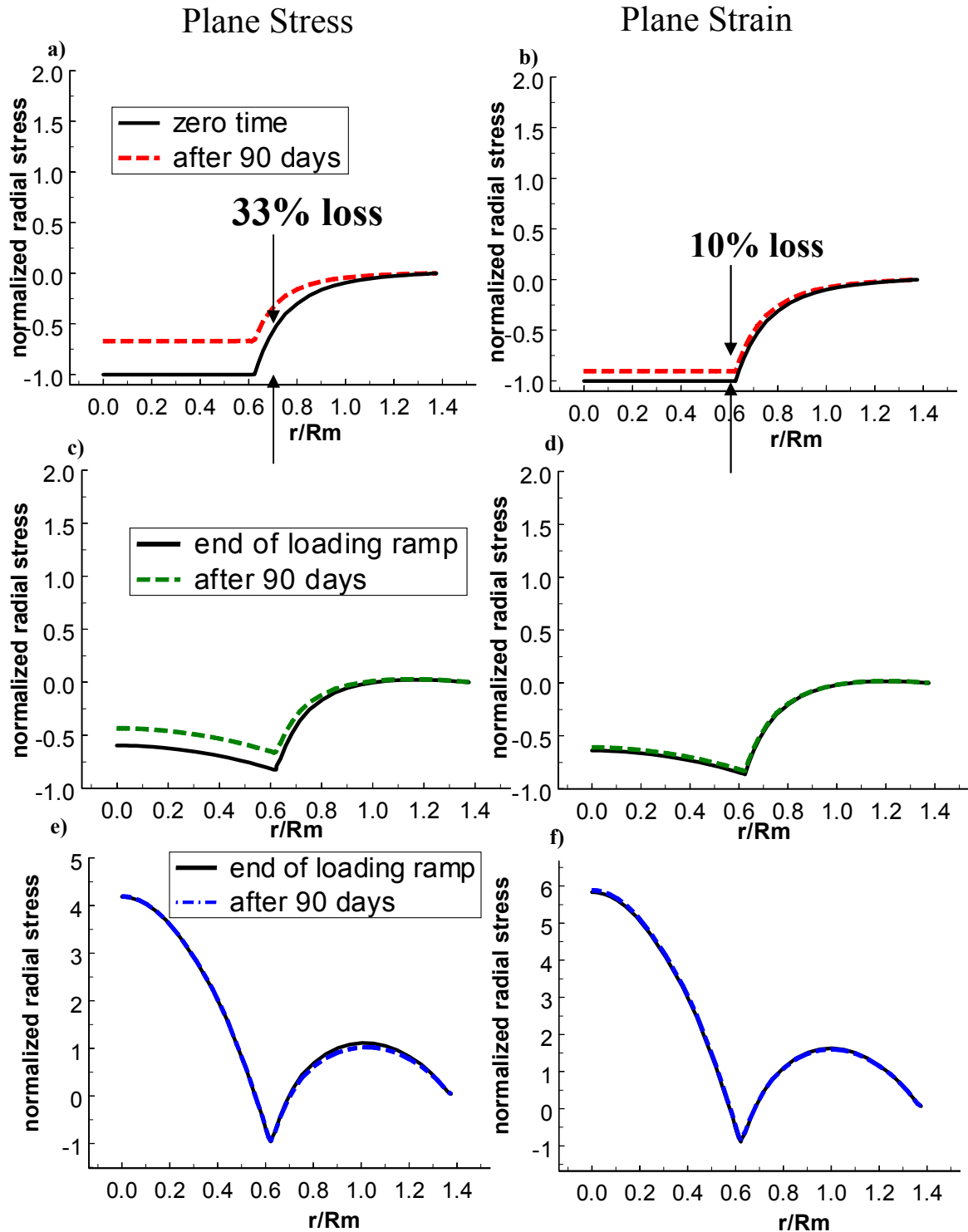


Figure 9 - A comparison between plane stress and plane strain conditions given a titanium hub- PMC rotor (7.62-cm radial thickness, $R_m=10.16$ cm) with a hoop prestrain of 0.5% subjected to three constant rotational speeds: 0 rpm (a and b), 20 Krpm (c and d) and 60 Krpm (e and f). The N.F.'s are: a) 141.62MPa, b) 155.68MPa, c) 142.72MPa, d) 156.03MPa, e) 57.43MPa and f) 45.99MPa, respectively. A viscoelastoplastic material representation was used in the analysis.

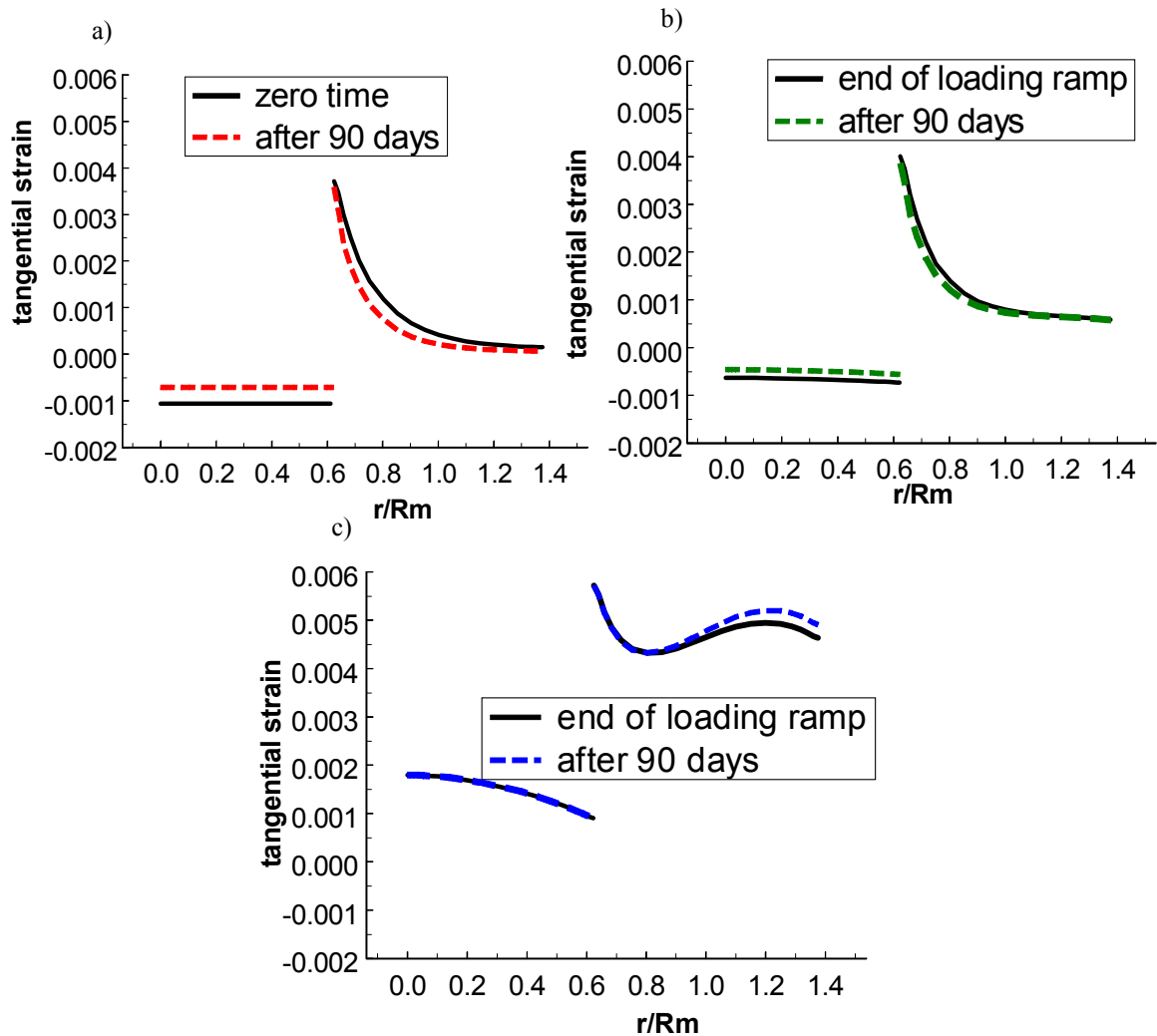


Figure 10 - Describes the tangential strain distribution within a thin (plane stress condition) titanium hub-PMC rotor (7.62-cm radial thickness, $R_m=10.16$ cm) with a hoop prestrain of 0.5% subjected to three constant rotational speeds using viscoelastoplastic representation; i.e., a) zero, b) 20 Krpm, and c) 60 Krpm.

Among different failure types that can occur, the burst failure criterion is one of the most stringent ones. Assuming that the fibers can stretch up to 1%, the tangential strain (which dictates the burst speed of the rim) indicates that for the more severe plane stress case, nearly 40 % of the allowable hoop strain is consumed during preloading (imposition of interference fit deformations) since no rotation is applied, see Fig. 10a. This amount increases to 42%, and 60% when 20 000 and 60 000 rpm rotational speeds are applied, respectively, see Fig. 10b and c. From the tangential strain distribution (Fig. 10), it is clear that the largest amounts of incremental changes in strain (with time) occurred near the *midsections* of the rim at *lower* speeds of rotations and shift gradually to the *outer* radius at *higher* speeds. Nevertheless, the highest magnitude of tangential strain remains at the location of the inner rim radius. Also, it is apparent from Fig. 10c that as the rotational speed is increased, the material throughout the rim is better utilized in that the material is more uniformly strained. This further illustrates the complex redistribution of stress and strain fields within the structure, which is only enhanced by time-dependent material behavior.

Material Gradation (Creep Mismatch)

A key motivation for the development of multi-disk rotors is the fact that at higher speeds of rotation the compressive stress due to hub/rim interference fit can be finally overcome such that a positive radial stress state is induced toward the middle of the rim. This positive radial stress, if excessive, could then cause delamination and/or failure of the rotor. This potential problem can be circumvented by introducing multiple sub-rims, which are in turn prestrained so as to maintain a compressive radial stress field *throughout* the rotor for all speeds of interest. Similarly, the associated hoop strain distribution is uniquely modified (so that a discontinuous stair step pattern is produced – with the highest hoop strain always occurring at the ID of the outer most rim) as a result of the multidisk configuration. To demonstrate the difference in radial stress and hoop strain distributions between a single disk and multidisk design (see Fig. 3a), the hub-PMC rotor configurations will be subjected to a 60 000 rpm constant rotation. Results are shown in Fig. 11, at the end of 10 days of operations. The analysis utilized a viscoelastoplastic material representation for the PMC rotor. Clearly, in the multidisk case, Fig. 11b, almost all-tensile radial stress is eliminated, except for a small region in the outer most disk, yet the influence of time dependency still persists. In fact it is enhanced over that of the single disk case, Fig. 11a, in that the amount of loss of preload (as compared to the time-independent, elastic, solution) is significant at the hub-rotor interface.

Figure 11 also clearly shows the classic discontinuous stair-step pattern (an artifact of this design and maintaining a compressive radial stress state throughout the rotor) for the hoop strain distribution in the multi-disk configuration as compared with the more uniform distribution given a single rotor disk. Obviously, the outer most disk is the most highly strained (which is deemed to be goodness from a fail-safe design standpoint) and therefore will be the first to experience burst due to an over load situation (see reference [1] for additional discussion regarding multi-disk design).

Another advantage of this multi-disk design is that it allows the possibility of introducing a different material for each disk within the rotor, i.e., the grading of the rotors' material properties, so that the influence of time-dependent behavior could be

potentially minimized. To study the influence of creep mismatch on the overall performance of the multi-disk design, the previous multidisk rotor design, with each subdisk having an interference fit of (0.5% r), was analyzed, see Fig. 3b. Each of the three rims was given new material properties (based on the original PMC material). For convenience, we define the three materials as follows; i.e., baseline (original IM7/8552, PMC) material as C_0 , a material with more tendency to creep (relative to the original), C_1 , and a third material, C_2 , with even more creep (relative to both C_0 and C_1) tendency. Three cases were analyzed using the following gradation schemes given these three materials, wherein each rim is assign a material from inner, to middle, to outer rim, respectively; i.e., case 1 (C_0, C_0, C_0), case 2 (C_0, C_1, C_2) and case 3 (C_2, C_1, C_0). All cases were subjected to the same constant speed of 60 000 rpm as previously analyzed using the viscoelastoplastic model.

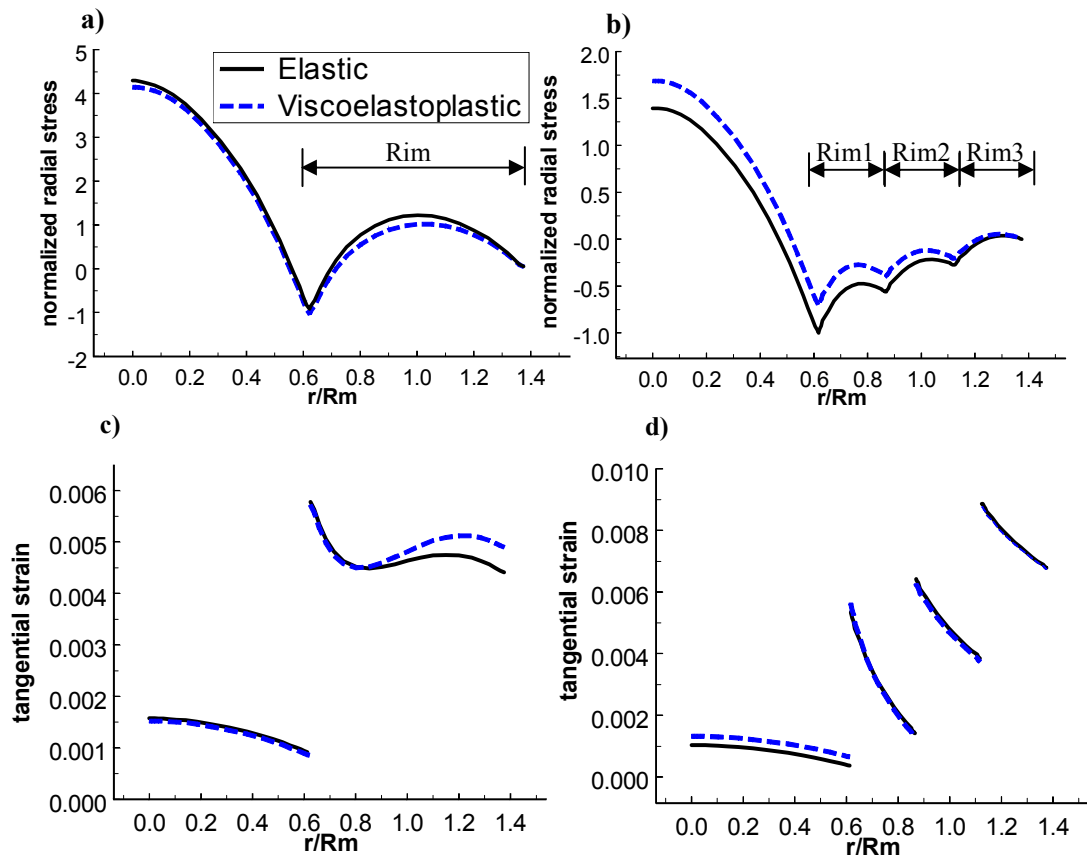


Figure 11- Normalized radial stress and tangential strain distributions (viscoelastoplastic analysis - PMC “material case 1”) of a preloaded configuration with a finite height (log): (a, c) single 7.62-cm thick rim and (b, d) three (each 2.54-cm) rims. The N.F. are 59.64 MPa for a) and 130.17 MPa for b). Stresses are normalized with respect to the elastic (time-independent) stress at the location of the hub-rotor interface. $R_m=10.16$ cm.

Results, in the context of normalized radial stress and hoop strain distributions are shown in Fig. 12 for all three cases. In Figure 12a it is clear that case 3 (where the inner rim exhibits the most time dependency) experiences a greater loss of preload than either of the other two cases, even though all three cases experience some time-dependency. Of course, this is not totally unexpected, and it hints at the fact that reducing the creep tendency in the inner ring (which could be accomplished by merely reducing the temperature at the hub/rotor interface given uniform material properties) will have the biggest effect in reducing the loss in preload pressure. An alternative approach is to use a more creep resistant matrix material within the PMC for the inner disk(s). It is interesting to note that the hoop strain distribution is hardly impacted by grading.

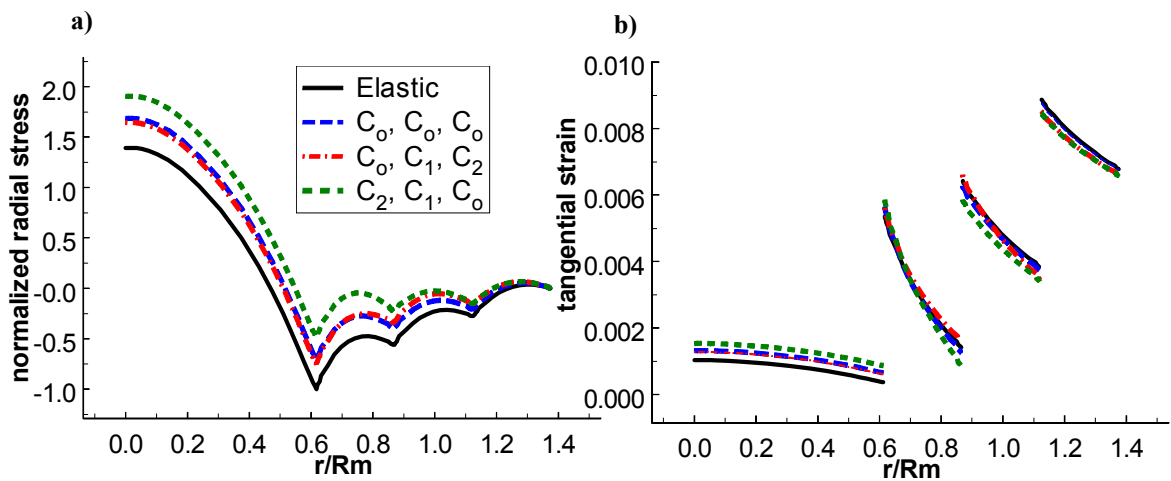


Figure 12- Influence of material gradation (creep mismatch) on the behavior of multidisk preloaded design using viscoelastoplastic analysis. Magnitude of misfit, at each interface, is equal to 0.5% times the radius at that interface. The three material cases are: case 1 (C_0, C_0, C_0), case 2 (C_0, C_1, C_2) and case 3 (C_2, C_1, C_0). The normalizing factor for the radial stress is, 130.17 MPa. The mean radius is 10.16 cm.

Analysis Results for MDC Design

In this design, reinforcement is now placed in both the radial and circumferential directions, thus producing a far more complex state of affair relative to the previous unidirectional preload design, since now anisotropy is severely impacting both in-plane and out-of-plane responses. The motivation for radial fiber placement stems from the desire to accommodate higher tensile radial stresses produced within a single, relatively thin (out-of-plane) and thick (in-plane) rotor. For this design, we will only examine a single loading case, i.e., a constant rotational speed of 60 000 rpm for 10 days. The same viscoelastoplastic material representation for the IM7/8552 PMC system, elastic titanium hub, interference fit between hub and rotor, and mean radius of 10.16 cm will

be utilized here to assist comparison of designs. It is important to realize that this configuration is not an optimal one (as for practical applications flexible composite hubs are being discussed), but rather just an example of an inexpensive certification test that might be conducted on a solid spin arbor. From our above material constraint study one might expect that minimal time dependency would be exhibited from this type of design since significant constraint is being introduced in both principal loading directions. As will be demonstrated, however, this is not the case, as significant time dependency is indeed observed. Stress and strain distribution results are shown (see Figs. 13 and 14) in the r - z plane via contour-type plots, while detailed distributions, at different instants of time, for representative circumferentially and radially reinforced layers (i.e., the fourth and fifth layers, respectively) will be displayed as a function of the normalized radius of the rotor. The stresses, reported are normalized with respect to their respective maximum values obtained from the *elastic (time-independent)* solution (at full speed) in each case.

5.1 In-Plane-Response

Referring to Figs. 13c, d, e and f, most of the time-dependent changes in the in-plane response components occur during the initial (60 minute) loading ramp. The radial stresses in the radially reinforced layers were significantly reduced (80% relaxation-at the center of the rotor) during the loading ramp, but later they slightly increase (0.7%) over the remaining 10 day period of constant loading, see Fig. 13c. This is in stark contrast with the response of the circumferentially reinforced layers where we observe approximately a 33% increase in radial stress (normal to the layer's fiber direction) during the loading ramp, and then an 11% reduction subsequently, see Fig. 13 d. The tangential strains in both the radial and circumferentially reinforced layers show similar behavior as they redistribute throughout the rotor thickness as compared to the elastic solution (approximately a 25% increase over 10 days toward the outer diameter), see Figs. 13e and f. Note that the circumferential layer is well within the allowable 1% fiber strain limit and the radial layer is within the transverse failure strain limit of 0.8%, see [20].

5.2 Out- of-Plane Response

Unique to the MDC design considered here, is the use of reinforcement in both principal directions. This is introduced through alternating layers of perpendicular fiber reinforcement producing inhomogeneous material properties in the out-of-plane direction. This inhomogeneity is reflected in significant interlaminar (out-of-the plane, r - z) shear stresses, which play a significant role in this type of design (e.g., may trigger a new delamination failure mode as compared with the previous preload design); see Fig. 14c. In Figs. 14a and b, contour plots of the transverse (r - z) shear stress and strain, respectively, distributions are shown. Note the existence of a region (near the interface of the hub-rotor) where the stresses and strains are highly concentrated. Also, the amount of change due to material time dependency in the transverse shear stress reaches a value of 230% (over that of the elastic analysis) in certain regions in the radially reinforced layers (between the middle of the rim and the ID). Furthermore, the

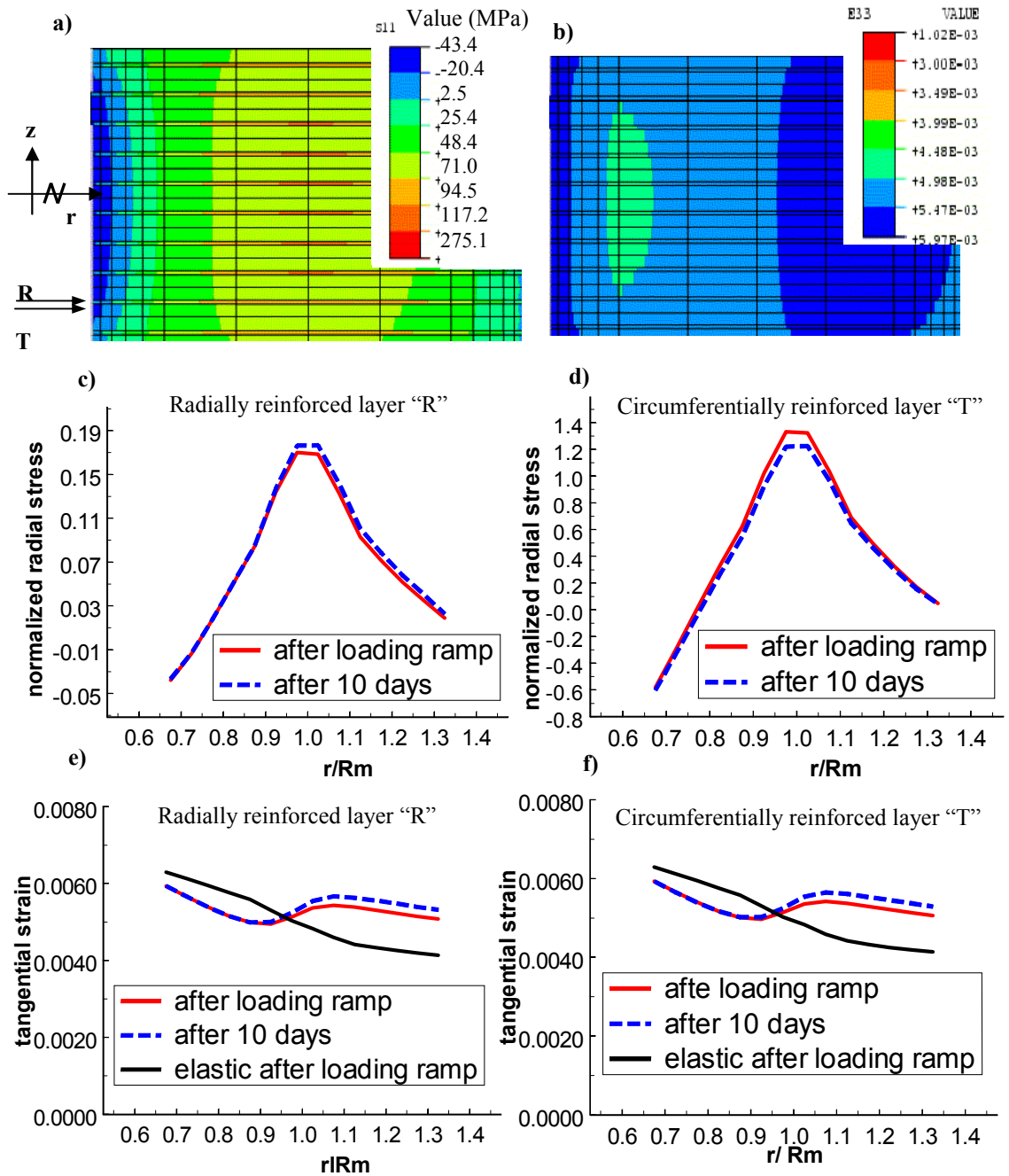


Figure 13 – Analysis of PMC MDC design subjected to 0.5% prestrain and 60 Krpm constant rotation using viscoelastoplastic model. Radial stress and tangential strain contours at the end of loading are shown in (a and b), respectively. Normalized radial stress and tangential strain in radially reinforced fifth layer and circumferentially reinforced fourth layer, are shown in, (c and e), and, (d and f), respectively. The stresses in (c and d) are normalized with respect to the corresponding maximum elastic stress at full speed. These factors are 535 MPa and 48.26 MPa, respectively. The mean radius is 10.16 cm.

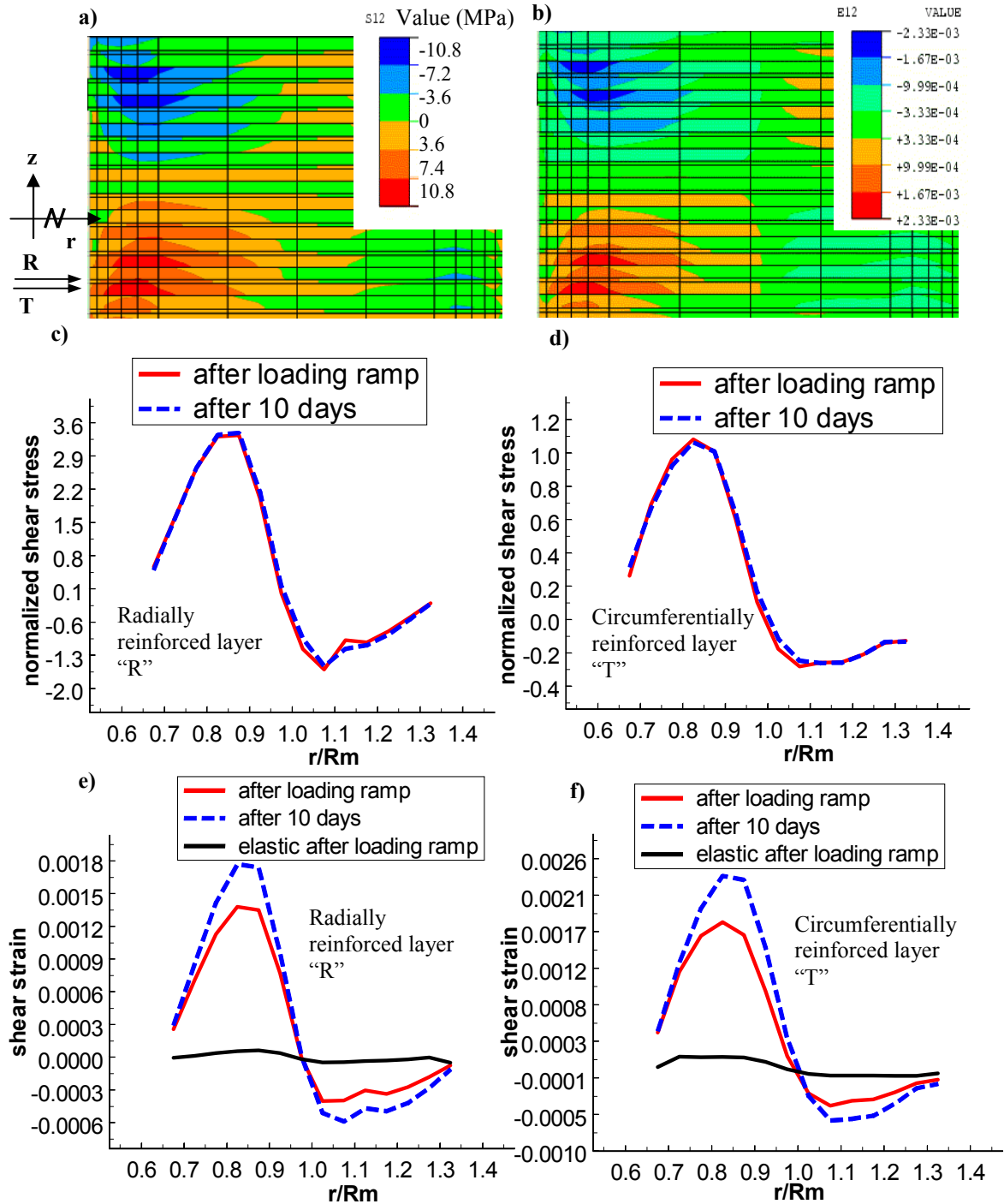


Figure 14 - Analysis of PMC MDC design subjected to 0.5% prestrain and 60 Krpm constant rotation using viscoelastoplastic model. Shear stress and shear strain contours at the end of loading are shown in (a and b, respectively). Normalized shear stress and shear strain in radially reinforced fifth layer and circumferentially reinforced fourth layer are shown in, (c and e), and, (d and f), respectively. The shear stresses in (c and d) are normalized with respect to the corresponding maximum elastic stress at full speed. These factors are 2.65 MPa and 10.62 MPa, respectively. The mean radius is 10.16 cm.

corresponding shear strains in these same regions of concentration continue to increase (creep) with time (see, Figs. 14e and f). With the actual values of shear strain, in the radially and circumferentially reinforced layers, reaching magnitudes of 0.18% and 0.24%, respectively, after 10 days of constant rotation at 60 000 rpm. Whether these magnitudes are approaching the limit of the material is not known at this time.

Remarkably, these latter significant changes and intense localizations for the transverse shear stress/strain components are unique to the plastic-type time dependency that is typical in viscoplasticity. Purely (linear) viscoelastic solutions will not exhibit this trend; in fact with the notion of viscoelastic bounds the distributions will remain identical to their elastic patterns in Figs. 14e and f (basically shifting up or down as a whole). In view of this marked differences between the two alternative material representations for the above “shear-type” response, it seems rather important that any experimental characterization test program should include shear-type tests. At present time, these are lacking for the PMC system considered here. The results in Fig. 14 are all based on the *predictive* capabilities of the viscoplastic model. Experimental confirmation (or other wise) of these trends would be very interesting, and should be a topic of future research.

Summary and Conclusions

As a main and general conclusion, both the preload (single or multidisk) and the MDC rotor designs will be significantly influenced by time-dependent material behavior, provided the application temperature is sufficient for the given material. Remember all results herein assumed an application temperature of 135°C, which produced a significant amount of time-dependent behavior in the PMC material system of interest. Clearly, this temperature is an upper use temperature and therefore the observed time-dependent behavior is an extreme example.

More specifically, the conclusions for each of the itemized aspects of this study can be summarized as follows (the first four were inferred from the study of both preload/and-MDC designs, and the fifth is unique to the current MDC rotor design)

Material Representations

- For Viscoelastic Solid Material (Pure Hardening)-Limit conditions exist and the mean cyclic and creep response (at this mean stress) are basically equivalent.
- For Viscoplastic Material- No limit state is readily available and the mean cyclic and creep response are not equivalent, as significant ratchetting behavior is predicted.
- Before any firm conclusion can be made, a cyclic PMC flywheel rotor test, at temperature, must be performed to verify the appropriate constitutive modeling approach (i.e., delineate between viscoelastic/viscoelastoplastic).

Material Constraints

- Fiber orientation can significantly impact the influence of time dependency
- Governing components (and thus failure mode) can shift from in-plane to out-of-plane.

Geometric Constraints

- Plane stress conditions typically exhibit more time dependency than do conditions of plane strain.
- The extent of these effects is a function of load level. For example, the most significant loss of preload occurs under no rotation, which implies that an assembled preloaded flywheel rotor should be stored in a controlled environment (cold) to ensure minimal loss of preload prior to use.

Material Gradation (Creep Mismatch)

- Influence of time-dependency can be increased or decreased depending upon the ordering of the material within the rotor.
- To minimize time-dependent behavior, a designer should place the least time dependent material toward the ID of the rotor. This gradation may also be achieved given the same material throughout, by introducing internal cooling.

MDC design

- Alternating layers with different preferred directions will induce inhomogeneity, thus causing the out-of-plane components (i.e., shear stress or shear strain) to become an important design factor.
- Further research and experimentation at the coupon level must be conducted on the out-of-plane shear response, to identify appropriate limit (failure) levels.
- Additionally, flywheel rotor experiments are needed to study the time variation response of MDC designs so as to enable firm conclusions to be made regarding the significance of time dependency in these flywheels.

References

- [1] Arnold, S. M., Saleeb, A. F., and Al-Zoubi, N. R., "Deformation and Life Analysis of Composite Flywheel Disk System," *Composites: Part B*, Vol. 33, 2002, pp. 433-459, and *NASA TM-2001-210578*, 2001.
- [2] Kossecki, J., "Generalized Plane State of Stress in Rotating Viscoelastic Disk with Elastic Loop," *Polska Akademia Nauk-rozprawy Inzynierskie*, Vol. 12, No. 2, 1964, pp. 297-307.
- [3] Ma, B., "Power-Function Creep Analysis for Rotating Solid Disks Having Variable Thickness and Temperature," *Journal Franklin Institute*, Vol. 277, No. 6, Jun, 1964, pp. 593-612.
- [4] Lenard, J., "Analysis of The Secondary Creep of a Rotating Flat Disk," *Transaction of Canadian Society of Mechanical Engineering*, Vol. 1, No. 4, 1972, pp. 227-228.
- [5] Gupta, S., "Analysis of Rotating Disk of Orthotropic Material in the Theory of Creep," *Institute of Engineering Journal (India)*, Mechanical Engineering Division, Vol. 58, pt ME 1, Jul, 1977, pp. 1-4.

- [6] Betten, J., and Shin, C., "Inelastic Behavior of Rotating Disks Considering Effects of Anisotropy and Torsorial Nonlinearity," *Forschung Ingenieurwesen*, Vol. 57, No. 5, Sep, 1991, pp. 137-147.
- [7] Gurvich, M., "Stress-Strain and Limit State Viscoelastic Chord Flywheel," *Probl. Prochn*, Vol. 6, Jun, 1987, pp. 7-11.
- [8] Trufanov, N., and Smetannikov, O., "Creep of Composite Energy Accumulators," *Strength of Materials*, Vol. 23, No. 6, Feb, 1992, pp. 671-675.
- [9] Emerson, R. P., and Bakis, C. E., "Relaxation of Press-Fit Interface Pressure in Composite Flywheel Assemblies," *43rd International SAMPLE Symposium*, May 31-June 4, 1998, pp. 1904-1915.
- [10] Emerson, R. P., and Bakis, C. E., "Viscoelastic Behavior of Composite Flywheels," *45rd SAMPLE Symposium and Exhibition*, May 21-25, Long Beach, CA, 2000, Society for the Advancement of Materials and Process Engineering, Covina, CA.
- [11] Tzeng J. T., "Viscoelastic Analysis of Composite Flywheels for Energy Storage," Army Research Lab, Aberdeen Proving Ground, MD 21005-5069, 2001.
- [12] Halpin, J. C., and Pagano, N. J., "Observations on Linear Anisotropic Viscoelasticity," *Journal of Composite Materials*, Vol. 2, No. 1, 1967, pp. 68-80.
- [13] Lou, Y. C., and Schapery, R. A., "Viscoelastic Characterization of a Non-Linear Fiber Reinforced Plastic," *Journal of Composite Materials*, Vol. 5, 1971, pp. 208-234.
- [14] Yeow, Y. T., Morris, D. H., and Brinson, H. F., "Time-Temperature Behavior of a Unidirectional Graphite/Epoxy Composites," *Composite Materials: Testing and Design (Fifth Conference)*, *ASTM STP 674*, American Society for Testing and Materials, Philadelphia, PA, 1979, pp. 263-281.
- [15] Tuttle, M. E., and Brinson, H. F., "Prediction of the Long Term Creep Compliance of General Composite Laminates," *Experimental Mechanics*, Vol. 26, 1986, pp. 89-102.
- [16] Sullivan, J. L., Blais, E. J., and Houston, D., "Physical Aging in the Creep Behavior of Thermosetting and Thermoplastic Composites," *Composite Science and Technology*, Vol. 47, 1993, pp. 389-403.
- [17] Hiel et al., "Nonlinear Viscoelastic Response of Resin Matrix Composite Laminates," *NASA CR 3772*.
- [18] Raghavan, J., and Meshii, M., "Prediction of Creep Rupture of Unidirectional Carbon Fiber Reinforced Polymer Composite," *Materials Science and Engineering A*, Vol. 197, 1995, pp. 239-249.
- [19] Brinson, H. F., "Matrix Dominated Time Dependent Failure Prediction in Polymer Matrix Composites," *Composite Structures*, Vol. 47, 1999, pp. 445-456.
- [20] Thesken, J. C., Bowman, C. L., Arnold, S. M., and Thompson, R. C., "Time-Temperature Dependent Response of Filament Wound Composites for Flywheel Rotors," *Composite Materials: Testing and Design Fourteenth Volume, ASTM STP 1436*, C.E. Bakis, Ed., ASTM International, West Conshohocken, PA, 2003. See also NASA TM-2003-212102.
- [21] Saleeb, A. F., and Arnold, S. M., "A General Reversible Hereditary Model: Part I: Theoretical Developments," *Journal of Engineering Materials and Technology*, Vol. 123, 2001, pp. 51-64.

- [22] Saleeb, A. F., Arnold, S. M., Castelli, M. G., Wilt, T.E., and Graf, W., "A General Hereditary Multimechanism-Based Deformation Model with Application to the Viscoelastoplastic Response of Titanium Alloys," *International Journal of Plasticity*, 17, 2001, pp. 1305-1350.
- [23] Arnold, S. M., Saleeb, A. F., and Castelli, M. G., "A General Reversible Hereditary Model: Part II: Application to a Titanium Alloy," *Journal of Engineering Materials and Technology*, Vol. 123, 2001, pp. 65-73.
- [24] Saleeb, A. F., Wilt, T. E., Trowbridge D. A., and Gendy, A.S., "Effective Strategy for the Automated Characterization in Complex Viscoelastoplastic Modeling for Isotropic/Anisotropic Aerospace Materials," *ASCE, Journal of Aerospace Engineering*, Vol. 15, No. 3, 2002, pp. 84-96.
- [25] Schapery, R. A., "Nonlinear Viscoelastic and Viscoplastic Constitutive Equations Based on Thermodynamics," *Journal of Mechanics of Time-Dependent Materials*, Vol. 1, 1997, pp. 209-240.
- [26] Veazie, D. R., and Gates, T. S., "Compressive Creep of IM7/K3B Composite and the Effects of Physical Aging on Viscoelastic Behavior," *Experimental Mechanics*, Vol. 37, No. 1, 1997, pp. 62-68.
- [27] Lamaitre, J., and Chaboche J. L., "*Mechanics of Solid Materials*", Cambridge University Press, 1990.
- [28] Onat, E.T., and Fardshisheh, F., "Representation of Creep of Metals", *Oak Ridge National Laboratory, ORNL-4783*, Aug, 1972.
- [29] ABAQUS standard, version 5.8, Hibbitt, Karlsson & Sorensen, Inc., Pawtucket, RI, USA. www.abaqus.com

REPORT DOCUMENTATION PAGE			Form Approved OMB No. 0704-0188	
Public reporting burden for this collection of information is estimated to average 1 hour per response, including the time for reviewing instructions, searching existing data sources, gathering and maintaining the data needed, and completing and reviewing the collection of information. Send comments regarding this burden estimate or any other aspect of this collection of information, including suggestions for reducing this burden, to Washington Headquarters Services, Directorate for Information Operations and Reports, 1215 Jefferson Davis Highway, Suite 1204, Arlington, VA 22202-4302, and to the Office of Management and Budget, Paperwork Reduction Project (0704-0188), Washington, DC 20503.				
1. AGENCY USE ONLY (Leave blank)		2. REPORT DATE January 2003		3. REPORT TYPE AND DATES COVERED Technical Memorandum
4. TITLE AND SUBTITLE A Study of Time-Dependent and Anisotropic Effects on the Deformation Response of Two Flywheel Designs			5. FUNDING NUMBERS WBS-22-755-12-11	
6. AUTHOR(S) Atef F. Saleeb, Steven M. Arnold, and Nasser R. Al-Zoubi				
7. PERFORMING ORGANIZATION NAME(S) AND ADDRESS(ES) National Aeronautics and Space Administration John H. Glenn Research Center at Lewis Field Cleveland, Ohio 44135-3191			8. PERFORMING ORGANIZATION REPORT NUMBER E-13743	
9. SPONSORING/MONITORING AGENCY NAME(S) AND ADDRESS(ES) National Aeronautics and Space Administration Washington, DC 20546-0001			10. SPONSORING/MONITORING AGENCY REPORT NUMBER NASA TM-2003-212091	
11. SUPPLEMENTARY NOTES Prepared for the 14th Symposium on Composite Materials: Testing and Design sponsored by the American Society for Testing and Materials, Pittsburgh, Pennsylvania, March 11-12, 2002. Atef F. Saleeb and Nasser R. Al-Zoubi, University of Akron, Civil Engineering Department, Akron, Ohio 44325; Steven M. Arnold, NASA Glenn Research Center. Responsible person, Steven M. Arnold, organization code 5920, 216-433-3334.				
12a. DISTRIBUTION/AVAILABILITY STATEMENT Unclassified - Unlimited Subject Category: 39 Available electronically at http://gltrs.grc.nasa.gov This publication is available from the NASA Center for AeroSpace Information, 301-621-0390.			12b. DISTRIBUTION CODE	
13. ABSTRACT (Maximum 200 words) The influence of material time dependency and anisotropy in the context of two specific flywheel designs—preload and multi-directional composite (MDC)—is investigated. In particular, we focus on the following aspects: 1) geometric constraints, 2) material constraints, 3) loading type, and 4) the fundamental character of the time-dependent response, i.e., reversible or irreversible. The bulk of the results presented were obtained using a composite (PMC IM7/8552 at 135 °C) material system. The material was characterized using a general multimechanism hereditary (viscoelastoplastic) model. As a general conclusion, the results have clearly shown that both the preload and the MDC rotor designs are significantly affected by time-dependent material behavior, which may impact the state of rotor balance and potentially reduce its operating life. In view of the results of the parametric studies and predictions made in the present study, the need for actual experimentation focusing on the time-dependent behavior of full-scale flywheel rotors is self-evident.				
14. SUBJECT TERMS Composite flywheel; Rotating disks; Deformation; PMC; Viscoplasticity; Viscoelasticity; Time-dependent material			15. NUMBER OF PAGES 33	
			16. PRICE CODE	
17. SECURITY CLASSIFICATION OF REPORT Unclassified	18. SECURITY CLASSIFICATION OF THIS PAGE Unclassified	19. SECURITY CLASSIFICATION OF ABSTRACT Unclassified	20. LIMITATION OF ABSTRACT	